



**Non-uniform distribution of dopant iron ions in TiO<sub>2</sub>  
nanocrystals probed by X ray diffraction, Raman scattering,  
photoluminescence and photocatalysis**

Journal:	<i>Journal of Materials Chemistry C</i>
Manuscript ID:	TC-ART-10-2014-002362.R2
Article Type:	Paper
Date Submitted by the Author:	21-Dec-2014
Complete List of Authors:	Manu, S; University of Kerala, Centre for Nanoscience and Nanotechnology Khadar, M. Abdul; University of Kerala, Centre for Nanoscience and Nanotechnology

## Non-uniform distribution of dopant iron ions in TiO<sub>2</sub> nanocrystals probed by X-ray diffraction, Raman scattering, photoluminescence and photocatalysis

S. Manu and M. Abdul Khadar\*

*Centre for Nanoscience and Nanotechnology, University of Kerala, Kariavattom,  
Thiruvananthapuram – 695581, Kerala, India*

\* Author to whom correspondence should be addressed: [mabdulkhadar@rediffmail.com](mailto:mabdulkhadar@rediffmail.com)

We have analyzed the experimental XRD patterns and micro-Raman spectra of iron doped nanocrystals of TiO<sub>2</sub> using model calculations and shown that the concentration of the dopant atoms near the surface of the TiO<sub>2</sub> nanocrystals is larger than that near the core due to a ‘self-purification mechanism’. A model for the observed decrease in the size of the iron doped nanocrystals of TiO<sub>2</sub> is offered based on the above mechanism. Photoluminescence spectra (PL) of the samples confirmed the location of oxygen vacancy levels resulting from iron doping. The rapid decrease in the photocatalytic activity of the samples with higher concentrations of dopant is attributed to an increased number of the dopant ions near the grain boundaries caused by self-purification. In this article we show that the phenomenon of ‘self-purification’ is a real mechanism operative in nanocrystals and that this should be taken into account while analyzing the properties of doped nanocrystals for practical applications.

### Introduction

Substitutional doping of bulk semiconductors for tuning their electronic properties has been the most important idea in the field of semiconductor science and technology that served as the basis for the development of the electronic industry. The revelation that the properties of semiconductors at nanometer dimensions, semiconductor nanocrystals, deviate markedly from their bulk properties prompted researchers to attempt doping as an additional handle for controlling the size dependant properties of nanocrystals further. Presently, the use of nanocrystals as materials for potential technological applications such as solar cells<sup>1</sup>, bio-imaging,<sup>2</sup> and tunable lasers<sup>3</sup> depends heavily on tailoring their properties through intentional doping with external impurities. TiO<sub>2</sub> is a strategic material for environmental photo-catalysis and photo-electrochemical solar-energy conversion<sup>4</sup> but, because of the wide band gap, this material can absorb only UV-radiation rendering the use of solar irradiation inefficient. One approach to increase the photo-activity of TiO<sub>2</sub> under the visible light is to directly modify the energy band of TiO<sub>2</sub> by doping of foreign atoms like iron (Fe). Different authors have

reported the study of Fe doped nanocrystals  $\text{TiO}_2$  to understand the modifications undergone by the  $\text{TiO}_2$  lattice and for using iron doped  $\text{TiO}_2$  for practical applications.<sup>5,6</sup> Several strategies have been implemented for the doping of nanocrystals.<sup>7,8</sup> George *et al.*<sup>9</sup> have reported the synthesis of Fe doped nanoparticles of  $\text{TiO}_2$  containing 1 – 10 wt% Fe homogeneously distributed in the  $\text{TiO}_2$  matrix by flame spray pyrolysis technique. Very recently, Li *et al.*<sup>10</sup> have reported the successive layer-by-layer doping method for homogeneous distribution of dopants in nanoparticles. In the present study, we have concentrated on the distribution of dopant iron ions in iron doped nanocrystals of  $\text{TiO}_2$  synthesized through chemical route. When a bulk semiconductor is under conditions of thermal equilibrium determined by Gibbs free energy and growth temperature, impurity atoms can be incorporated up to their solid solubility limit which is as much as 50% or more, for example, for Mn in II-VI semiconductors.<sup>11</sup> But, doping of nanocrystals has been demonstrated to be a difficult process<sup>12,13</sup> Erwin *et al.*<sup>14</sup> suggested that the difficulties encountered in doping nanocrystals are due to the reason that the mechanism of impurity doping in bulk materials and in nanocrystals are greatly different while other worker attributed this difficulty to ‘self-purification’ mechanism<sup>15</sup> which hampers the introduction of defects at the nanoscale and by which impurities are expelled. Although significant progress has been reported in recent years in doping nanocrystals of II-VI<sup>16,17</sup> and other materials,<sup>18,19</sup> the degree of doping achieved so far at the nanoscale is far lower than that expected from the thermodynamic limit and for some materials is even zero. Norris *et al.* have reviewed the advances in the synthesis and theoretical understanding of the mechanism controlling doping of nanocrystals<sup>20</sup> and Cao has recently discussed the role of impurity doping in enhancing the performance of semiconductor nanocrystals in electronic devices.<sup>21</sup> Incorporation of even a single impurity atom into a semiconductor nanocrystal of diameter about 5 nm is equivalent to a dopant concentration of  $\sim 10^{19} \text{ cm}^{-3}$  which is in the limit of extremely heavy doping in the case of a bulk semiconductor.<sup>22</sup> As a result, while dopant atoms are considered to be uniformly distributed in bulk crystals, their distribution in nanocrystals may be grossly non-uniform.

Mocatta *et al.*<sup>23</sup> have argued that even though impurity atoms can reside on the surface of nanocrystals, only the dopants inside the nanocrystals have a role in determining the electronic properties of these nanocrystals. A few experimental techniques like optical absorption,<sup>24</sup> ESR<sup>25</sup> and magnetic circular dichroism<sup>16, 17</sup> have been demonstrated to be capable of distinguishing dopants residing on the surface of nanocrystals from those inside. Sharma *et al.* have indicated that a decrease in the ratio of intensity of XRD peaks of Mn

doped TiO<sub>2</sub> thin films were due a change in the structure factor due to Mn doping<sup>26</sup>. In the present work, we have synthesized Fe doped nanocrystals of TiO<sub>2</sub>, Ti<sub>(1-x)</sub>Fe<sub>x</sub>O<sub>2</sub>, containing different atomic ratio (x) of Fe using a method which is a modification of the method reported by Lei Ge *et al.*<sup>27</sup> The as-prepared powder samples are annealed at 600°C/800°C for 1 hour to obtain nanocrystalline Fe doped TiO<sub>2</sub>. The results of EDS analysis showed that a major part of iron in the starting solution got incorporated into the nanocrystals of TiO<sub>2</sub>. We have analyzed the XRD patterns and micro-Raman spectra of Fe doped nanocrystals of TiO<sub>2</sub> using model calculations and shown that the concentration of the dopant atoms near the surface of the TiO<sub>2</sub> nanocrystals is larger than that at the core due to a ‘self-purification mechanism’. A model for the observed decrease in the size of the Fe doped nanocrystals of TiO<sub>2</sub> is offered based on the above mechanism. Photoluminescence spectra of the samples confirmed the location of oxygen vacancy levels resulting from Fe doping. The photocatalytic efficiency of the iron-doped nanopowders of TiO<sub>2</sub> was evaluated from the photocatalytic decomposition of aqueous solution of methylene blue containing the suspended photocatalyst under visible light irradiation. The degradation of methylene blue was greatest when 1 atom % Fe doped nanoparticles of TiO<sub>2</sub> was used as the catalyst and the degradation decreased with increase in the doping percentage of iron. TiO<sub>2</sub> nanocrystals containing 25 atom % of Fe did not show any significant photocatalytic activity. The rapid decrease in the photocatalytic activity of the samples with higher concentrations of dopant iron is attributed to an increased concentration of the dopant near the grain boundaries caused by self-purification. In this article, we show that the phenomenon of ‘self-purification’ is a real mechanism operative in nanocrystals and that this should be taken into account while analyzing the properties of doped nanocrystals for practical applications.

## Results and discussion

### X-ray diffraction studies

The XRD pattern of the un-doped sample F0 (The digit after F indicate atom percentage of Fe) in Fig. 1 shows peaks of only anatase phase of TiO<sub>2</sub>. The XRD patterns of F1, F2, F5, and F8 (The digit after F indicate atom percentage of Fe) are identical with the pattern of F0, except for a conspicuous decrease in the intensity of the peaks, showing that doping of TiO<sub>2</sub> with iron up to atom % of 8 did not cause a change of phase from anatase or amorphisation of the lattice and that the iron atoms got incorporated at lattice positions of TiO<sub>2</sub>.

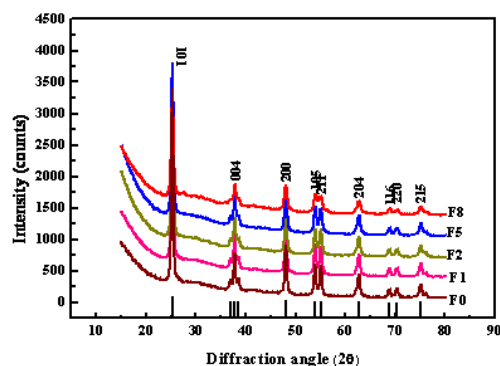


**Fig. 1** X-Ray diffraction patterns of samples F0, F1, F2, F5, and F8.

But the samples F15, F20\*, and F25\* gave XRD patterns<sup>28</sup> completely different from the pattern of the undoped sample F0 or of the samples F1, F2, F5, and F8. The asterisk represents samples annealed at 800°C. The samples without asterisk represent samples annealed at 600°C. All the XRD peaks of F15 except the one at 2θ value of 25.3° which is the strongest (101) peak of anatase phase, are associated with rutile phase of TiO<sub>2</sub>. Nanocrystalline TiO<sub>2</sub> samples doped with 20 and 25 atom % of Fe and annealed at 600°C had amorphous structure.<sup>28</sup> But when the two samples are annealed at 800°C for 1 hour (F20\* and F25\*), the XRD patterns showed peaks of F15 along with new peaks.<sup>28</sup> All the new peaks in the XRD patterns of F20\* and F25\* are identified as peaks belonging to iron titanium oxide (pseudobrookite).

The intensity of any XRD peak which corresponds to reflection from a set of (hkl) planes is determined by the atomic scattering factor ( $f_N$ ) of the atoms lying in those planes and their relative positions according to the structure factor (F) given by<sup>29</sup>

$$F_{hkl} = \sum_N f_N \exp[2\pi i(hu_N + kv_N + lw_N)]. \quad (1)$$

where  $u_N, v_N, w_N$  are the fractional coordinates of the atoms and N represents the different types of atoms (ie., Ti, Fe and O) in a unit cell of Fe doped TiO<sub>2</sub>. The intensity of the XRD peaks of nanocrystals of Fe doped TiO<sub>2</sub> compared to that of un-doped TiO<sub>2</sub> nanocrystals was found to progressively decrease with increase in the doping percentage of Fe.<sup>28</sup>

The intensity of XRD peak is proportional to the square of the modulus of the structure factor. Making use of eqn. (1), we modelled the intensity,  $I$ , of the XRD peaks of Fe doped nanocrystals of TiO<sub>2</sub> as a function of the atomic ratio,  $x$ , of Fe as

$$I = [Af_1(1-x) - Bf_2x]^2. \quad (2)$$

where  $f_1$  and  $f_2$  are the atomic scattering factors of Ti and Fe respectively, and  $A$  and  $B$  are parameters to be determined through curve fitting of eqn. (2) to the experimental XRD data. The contribution to the intensity by the oxygen atoms is ignored in eqn. 2, since the atomic scattering factor of oxygen is small. The Fig. 2 shows the fitting of eqn. (2) to the experimentally obtained intensities of the strongest XRD peak (101) of the Fe doped nanocrystals of TiO<sub>2</sub>. The data points for atom % of Fe larger than 8 are excluded from Fig. 1 due to the partial phase change of nanocrystals of TiO<sub>2</sub> for higher concentrations of Fe. The values of the parameters  $A$  and  $B$  obtained by fitting the eqn. (2) to the experimental data points in Fig. 1 by putting the value of  $f_1$  as 22 and that of  $f_2$  as 26 are  $2.733 \pm 0.058$  and  $5.280 \pm 1.273$  respectively. The effect of the larger value of  $B$  is to increase the value of  $x$  so that the phase of waves scattered from Fe atoms are sufficiently out of phase with those from Ti atoms resulting in a decrease in the intensity as obtained in the experiment. If we assume that the effect of the large value of  $B$  is to increase the concentration of Fe atoms throughout the nanocrystals, then this assumption will have no physical basis and would turn out to be simply a convenient assumption to satisfy the eq. (2). But, due to the high local energy associated with the dopants, nanoparticles always have a tendency to expel impurity atoms because of thermodynamic requirement of minimizing the energy of the system, which is the self purification mechanism,<sup>15</sup> and as a result the concentration of dopant atoms near the surface could always be greater than that near the core of the nanocrystals. Hence the larger value of  $B$  in the present case can be considered to be a representation of the larger concentration of iron, than that represented by the  $x$  values, near the surface of the nanocrystals. It is also inferred from the regular decrease of the XRD peak intensity that Fe is

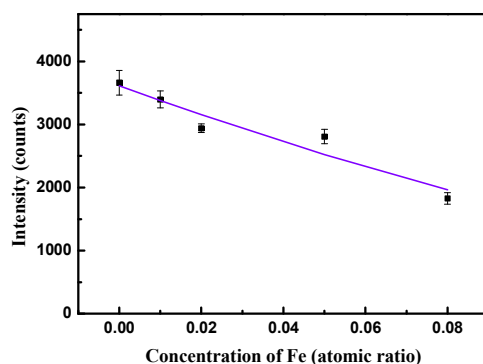


**Fig. 2** Variation of intensity of the most intense (110) peak in the XRD patterns of Fe doped TiO<sub>2</sub> nanocrystals with atomic ratio of Fe (dark spots) showing the fit (continuous line) of eq.2 to the experimental intensity.

incorporated by substitutional doping for Ti in the lattice planes rather than through interstitial occupation.

The grain sizes of the un-doped and Fe doped nanocrystals of TiO<sub>2</sub> are calculated using the FWHM of the (101) peak of anatase and (110) peak of rutile phases of TiO<sub>2</sub> employing Scherrer equation.<sup>29</sup> Fig. 3 shows that the grain size of the iron doped nanocrystals of TiO<sub>2</sub> decreased with increase in iron content in the samples. Transmission electron microscope images of F1 and F2<sup>28</sup> show nanocrystals with sizes agreeing fairly well with the crystallite sizes estimated from line broadening of the XRD peaks (~20 nm). A decrease in the size of nanocrystals on doping was observed in several cases including Fe doped TiO<sub>2</sub> nanocrystals.<sup>30,31</sup> The reduction in the size of Fe doped nanocrystals of TiO<sub>2</sub> was interpreted as due to the substitutional doping of Fe<sup>3+</sup> ions of lower ionic radius for Ti<sup>4+</sup> ions in the anatase and rutile structures.<sup>32</sup> We offer an explanation based on growth kinetics and self purification mechanism for the observed decrease in size of Fe doped nanocrystals of TiO<sub>2</sub> with increase in the doping % of Fe. Precipitation of nanocrystals from solutions is a two step process. During the first step, critical nuclei of the material are formed which grow subsequently to nanocrystals in the second step. Nucleation, in general, is homogeneous and the growth rate of the nanocrystals is controlled by poly-nuclear growth mechanism for mono-sized particles.<sup>33</sup> The rate of crystallization ( $R$ ) can be expressed in terms of the semi-empirical kinetics equation

$$R = kf(s)\sigma. \quad (3)$$

where  $k$  is the rate constant for crystal growth,  $f(s)$  is a function of the total number of available growth sites on the growing nanocrystals and  $\sigma$  the relative super saturation equal to  $(C-C_\infty)/C_\infty$ ,  $C$  and  $C_\infty$  being the solute concentration in solution and at equilibrium respectively.<sup>34</sup>  $f(s)$  should have a maximum value when the growth sites are provided by the host atoms and should decrease with increase in the number of dopant atoms near the growth sites. Under poly-nuclear growth process, the particles grow linearly with time ( $t$ ) so that the radius ( $r$ ) is given by

$$r = r_0 + k_p t. \quad (4)$$

where  $r_0$  is the initial size of the nucleus,  $k_p$  is a constant dependant only on temperature.<sup>31</sup> Making use of eqn. (3) and (4), we modelled the size of the nanocrystals as a function of atomic ratio  $x$  of dopant as:

$$\begin{aligned} r &= r_0 - kf(s)x \quad \text{or} \\ r &= r_0 - Dx. \end{aligned} \quad (5)$$

where  $D$  is a parameter to take into account the negative rate of growth of the nanocrystals due to the decrease in available growth sites as a result of the incorporation of dopant atoms. Fig. 3 shows the fitting of equation (5) to the experimental variation of size of the nanoparticles with doping concentration ( $x$ ) of Fe.

The agreement between the experimental data points and simulated curve is an indication of the validity of the argument that the decrease in the size of the Fe doped nanocrystals of  $\text{TiO}_2$  is due to the reduced number of growth sites with increase in the Fe doping concentration. Erwin *et al.*<sup>14</sup> have clearly demonstrated that for the incorporation of impurities into a nanocrystal, they should bind to its surface for a residence time comparable to the reciprocal growth rate and the binding energy of an impurity adsorbed on a given facet determines its residence time. In the case of growth of nanocrystals of  $\text{TiO}_2$ , the binding energy for Ti and oxygen ions on a growing nucleus will be maximum on surfaces containing these ions only and the presence of Fe ions on a surface will reduce the binding energy for Ti or oxygen ions on that surface. The value of  $D$  obtained though the fitting procedure was  $79.549 \pm 6.280$ . A value of  $D$  larger than unity in eq. (5) has to be considered as a representation of an increase in the concentration of Fe near surface of the  $\text{TiO}_2$  nanocrystals

since the increase in the value of  $x$  uniformly throughout the nanoparticles has no physical basis, while increase in the concentration near the grain boundaries has physical reason based on self purification mechanism. The increase in the effective value of ' $x$ ', on and near the growth surface of the nanocrystals results in a decrease of their size.

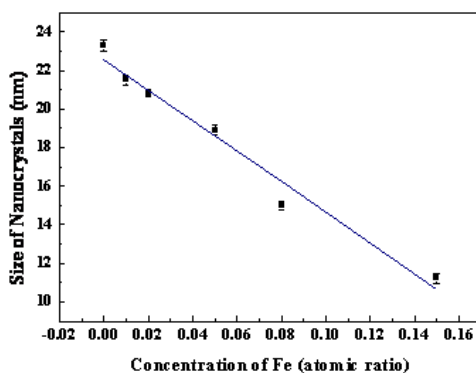


**Fig. 3** Size of iron doped nanocrystals of  $\text{TiO}_2$  as a function of atomic ratio of iron. Dark spots represent experimental points. Continuous line represents the fit of eq.5 to the experimental data.

### Micro-Raman studies

The micro Raman spectra of F0, F1, F2, F5 and F8 are shown in Fig. 4 and those of F15, F20\* and F25\* are given in<sup>28</sup>.

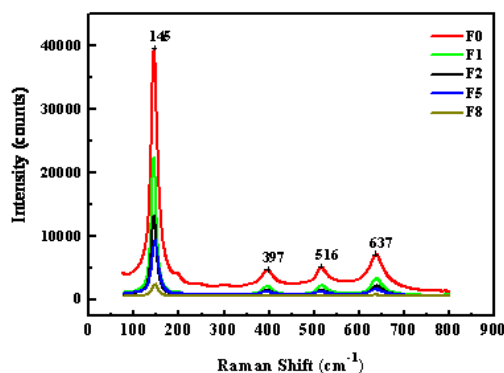


**Fig. 4** Micro-Raman spectra of samples F0, F1, F2, F5 and F8.

The spectra of samples F0, F1, F2, F5 and F8 exhibit characteristic Raman peaks of anatase phase of  $\text{TiO}_2$ <sup>35</sup> at 145, 197, ~397, ~517 and ~638  $\text{cm}^{-1}$ . The spectrum of F15 showed an

amorphous pattern<sup>28</sup> with peaks not well formed but with the most intense Raman line of anatase appearing around  $150\text{ cm}^{-1}$ . The spectra of F20\* and F25\* are totally different from those of F0 or of the doped samples containing smaller concentrations of Fe indicating the formation of the phase identified as iron titanium oxide from the XRD pattern<sup>28</sup> and the characteristic Raman peaks appearing at 199, 222, and  $335\text{ cm}^{-1}$ .<sup>36</sup> Fig. 4 and<sup>28</sup> show that the intensity of the peaks decreased rapidly with increase in the atom % of iron in the samples.

The vibrational modes of a crystal or molecule will appear as peaks of different intensity in its Raman spectrum. The intensity  $I_i$  of the  $i^{\text{th}}$  fundamental mode of vibration characterized by the normal coordinate  $Q_i$  may be written based on Placzek's simplified polarizability theory<sup>37</sup> as

$$I_i \propto \left( \frac{\partial \alpha}{\partial Q_i} \right)^2. \quad (6)$$

where  $\alpha$  is the molecular polarizability. Equation (6) shows that molecules or classes of compounds with small values of molecular polarizability would give Raman spectra with only low overall intensity, assuming that with small  $\alpha$  the changes  $\frac{\partial \alpha}{\partial Q}$  would also be small.

The intensity,  $I$ , of the Raman lines of the doped samples can be modelled as a function of the atomic ratio,  $x$ , of dopant as

$$I = I_0 (1 - Ex)^2. \quad (7)$$

where  $I_0$  is the intensity due to undoped nanocrystals of  $\text{TiO}_2$  and  $E$  is a parameter to indicate the actual concentration of the dopant Fe ions near the surface of the  $\text{TiO}_2$  nanocrystals. Fig. 5 shows the fitting of the eqn. (7), considering it as a second order polynomial, to the intensity of the most intense line in the Raman spectra of the  $\text{TiO}_2$  nanocrystals for different atomic ratio of Fe.

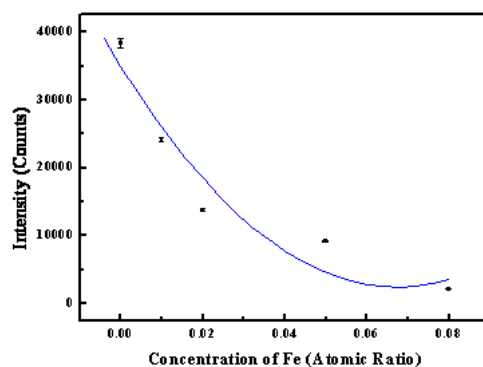


**Fig. 5** Variation of intensity of the strongest Raman peak of the Fe doped TiO<sub>2</sub> nanocrystals with atomic ratio of Fe (dark spots) along with fit (continuous line) of eq. 7.

Similar fitting can be done for the variation of intensities of the other Raman lines in the spectra. The effect of a large value of the parameter  $E$  (value of  $E$  obtained was nearly 14) in eqn. (7) has to be interpreted as a representation of an effective larger value of  $x$  near the surface of the nanocrystals due to self purification mechanism, since an increase in the value of  $x$  throughout the nanocrystals cannot be assumed. As in case of the results from XRD, we take the regular decrease in the intensity of the Raman lines with increase in the doping % of Fe to infer that the dopant Fe atoms are substitutionally incorporated into the host lattice rather than occupying interstitial positions.

### Optical absorption and photoluminescence

Doping of TiO<sub>2</sub> with Fe generates oxygen vacancies to maintain charge neutrality and the average number of oxygen vacancies is half the number of dopant atoms.<sup>38</sup> The energy levels associated with the oxygen vacancies will be deepest in the band gap of TiO<sub>2</sub> nanocrystals when the dopant Fe ions are most tightly bound to the host TiO<sub>2</sub> lattice which will happen when the Fe ions are substituted for Ti ions in the lattice planes of TiO<sub>2</sub>. The optical absorption of the Fe doped TiO<sub>2</sub> nanocrystals derived from diffuse reflectance spectra showed a regular shift of the absorption edge towards longer wave lengths as doping concentration of Fe is increased.<sup>28</sup> The decrease in band gap energy of the samples with increase in the atom % of Fe is a result of the introduction of new energy levels in the band gap. The band gap is the smallest for the doped sample containing the highest concentration of Fe (F25\*). The Photoluminescence spectra spectrum of F0 in Fig. 6 shows five emission

peaks centered at 2.63, 2.74, 2.95, 3.09 and 3.24 eV. The peak at  $\sim 3.24$  eV arises out of band edge emission while the peaks at 3.09 and 2.95 eV originate from charge recombination on the shallow-trap surface states. The peaks at 2.74 and 2.63 eV are due to oxygen vacancies.<sup>39,40</sup> As the dopant concentration increased, the intensity of the peaks except that of the peak at 2.63 eV decreased, may be due to Fe-Fe interactions acting as luminescence quencher as in the case of Eu doped TiO<sub>2</sub> nanoparticles,<sup>41</sup> and in the spectrum of F25\*, only the peak at 2.63 eV is visible. This observation shows that the energy level associated with the peak at 2.63 eV is the deepest defect related level and the Fe ions responsible for the

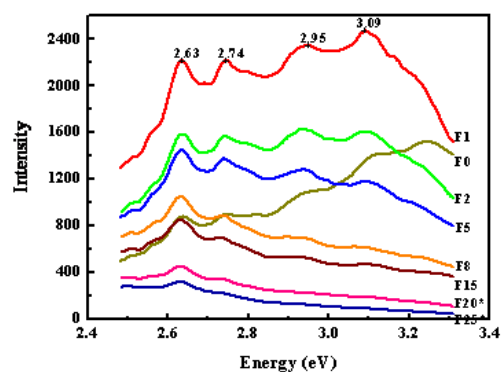


**Fig. 6** Photoluminescence spectra of samples F0 to F25\*.

creation of this level are incorporated at substitutional positions in the lattice in agreement with XRD and micro-Raman results.

### Photocatalysis

The intensity of absorbance peak ( $A$ ) of the methylene blue (MB) dye solution, located at 664 nm, was taken as a measure of the residual concentration of MB dye. The normalized residual concentration of MB dye was then obtained using the relation:

$$C/C_0 = A/A_0$$

where  $C$  is the concentration corresponding to the absorbance  $A$  at any particular time and  $A_0$  is the absorbance of the MB solution prior to the addition of photocatalyst corresponding to the initial MB dye concentration ( $C_0$ ).

The variations of residual MB concentration as a function of irradiation time are shown in Fig. 7.

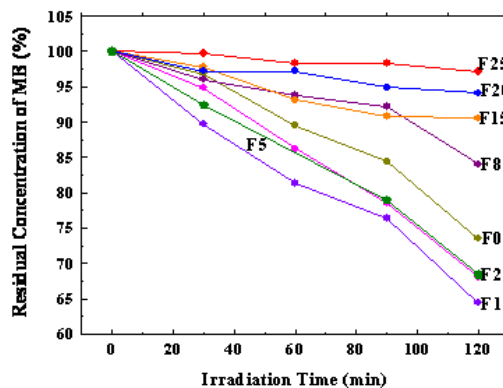


**Fig. 7** Residual normalized concentration of methylene blue vs visible light irradiation time in presence of undoped and 1, 2, 5, 8, 15, 20 and 25 atom % Fe-doped TiO<sub>2</sub> nanocrystals.

The degradation of MB was greatest for 1 atom % Fe doped nanoparticles of TiO<sub>2</sub> and it decreased with increase in the doping percentage of iron. TiO<sub>2</sub> nanocrystals containing 25 atom % of Fe did not show any significant photocatalytic activity. The photocatalytic activity exhibited by the undoped TiO<sub>2</sub> was lower than that for 1 atom % Fe-doped TiO<sub>2</sub> nanoparticles.

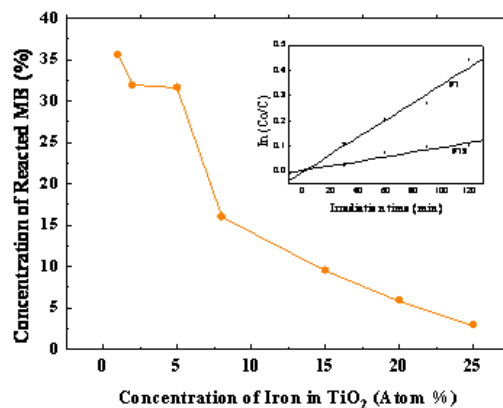


**Fig. 8** Plot of concentration of reacted MB solution after two hours of visible light irradiation against concentration of iron ions in TiO<sub>2</sub> (Atom %). Inset shows the rate constant graphs for degradation of MB for 1 atom % and 15 atom % Fe-doped TiO<sub>2</sub> nanoparticles.

The photocatalytic activity of TiO<sub>2</sub> originates from the production of excited electrons ( $e^-$ ) in the conduction band, along with holes ( $h^+$ ) in the valence band through the absorption of light of appropriate wavelength. These charge carriers may be used up through different paths.<sup>42</sup> First, they can get trapped either in shallow traps or in deep traps in the band gap of TiO<sub>2</sub>.

Secondly, they can recombine, non-radiatively or radiatively, dissipating the input energy as heat. Finally, they can react with electron donors or acceptors adsorbed on the surface of the photocatalyst resulting in their degradation.<sup>43</sup> In nanoparticles, most charge-carriers are generated close to the surface so that they may quickly reach the surface and undergo rapid surface recombination.<sup>44</sup> The surface carrier recombination is much faster than the interfacial charge carrier transfer process. The photocatalytic efficiency of TiO<sub>2</sub> can be improved by reducing the electron-hole recombination rate. Iron doping in nanocrystalline TiO<sub>2</sub> yields two opposite effects. The positive effect is that an increase in trapping sites through iron doping leads to effective trapping of the charge carriers. The negative effect is that the increased number of trapped charge carriers results in shorter lifetimes for interfacial charge transfer. The photocatalytic degradation of MB solution under the action of TiO<sub>2</sub> nanocrystals doped with iron of different atom % was found to satisfy the first-order rate equation given by:

$$C = C_0 \exp (-kt)$$

where  $k$  is the reaction rate constant and  $t$  is the time.

The PL spectra (Fig. 6) of the undoped and Fe doped nanoparticles of TiO<sub>2</sub> show that the intensity of the peaks except that of the peak at 2.63 eV associated with the deepest defect related level decreased with atom % of dopant Fe and finally these peaks disappeared. The disappearance of the defect levels from the band gap of the nanoparticles of TiO<sub>2</sub> would result in a decrease in the trapping sites for charge carriers and thereby accelerate the electron-hole recombination and cause a decrease of the photocatalytic activity. The photocatalytic activity of the Fe doped nanocrystals of TiO<sub>2</sub> was found to decrease rapidly with increase in the concentration of the dopant as shown in Fig. 8 and from the much reduced value of rate constant (0.0009 s<sup>-1</sup>) of F15, for example, compared to the value (0.0035 s<sup>-1</sup>) for F1 (inset to Fig. 8). The rapid decrease in the photocatalytic activity of the samples for higher concentrations of dopant is attributed to an increased number of the dopant ions near the grain boundaries caused by self-purification.

## Conclusion

In conclusion, we have shown through an analysis of XRD and micro-Raman data that in Fe doped nanocrystals of TiO<sub>2</sub>, the concentration of dopant is more near the grain boundary due to 'self purification mechanism' and that the dopant atoms are incorporated in the lattice at substitutional positions. Atom % dopant and crystallite size are smoothly correlated in the present study. PL spectra of the samples have shown that the energy level associated with the peak at 2.63 eV is the deepest defect related level and the iron ions responsible for the

creation of this level are incorporated at substitutional positions in the lattice in agreement with XRD and micro-Raman results. The rapid decrease in the photocatalytic activity of the samples with higher concentrations of dopant is attributed to an increased number of the dopant ions near the grain boundaries caused by self-purification. In this article we have shown that the phenomenon of 'self-purification' is a real mechanism operative in nanocrystals and that this should be taken into account while analyzing the properties of doped nanocrystals for practical applications.

## Experimental

The method reported by Lei Ge *et al.*<sup>27</sup> with modification was adopted in the present study for synthesizing nanocrystals of TiO<sub>2</sub> doped with Fe at different atomic ratios. Nanocrystals of TiO<sub>2</sub> were prepared from titanyl sulphate (TiOSO<sub>4</sub>.xH<sub>2</sub>O, Riedel-de-Haen, Germany) and iron doped nanocrystals of TiO<sub>2</sub> were synthesized from titanyl sulphate and ferrous sulphate (FeSO<sub>4</sub>.7H<sub>2</sub>O, Merck, India). To prepare undoped nanocrystalline TiO<sub>2</sub>, 10.34 g of titanyl sulphate was dissolved in 200 ml of distilled water. To this solution, a solution of 12 ml of 30% ammonium hydroxide in 50 ml of distilled water was dropped with vigorous stirring using a magnetic stirrer. The white precipitate formed was washed repeatedly with distilled water to remove the by-products of the precipitation reaction. The precipitate was then peptized in 40 ml of 30% H<sub>2</sub>O<sub>2</sub> diluted to 200 ml with distilled water. A yellow gel of peroxo titanate acid formed in half an hour. The gel was dried in an oven at 150°C for 4 hours and the dried mass was ground to a fine powder using an agate mortar and pestle. The powder was then annealed at 600°C for 1 hour to get the nanocrystalline TiO<sub>2</sub>. Iron doped nanocrystals of TiO<sub>2</sub> were synthesized through a similar procedure as above with ferrous sulphate (FeSO<sub>4</sub>.7H<sub>2</sub>O) of appropriate quantity added to titanyl sulphate before dissolving it in water. Seven samples of nanocrystals of TiO<sub>2</sub> doped with iron at atomic ratios from 1 to 25 were prepared. The samples were assigned the sample codes F0, F1, F2, F5, F8, F15, F20, F20\*, F25 and F25\* where the number after F denotes the doping percent of iron and the \* indicates samples annealed at 800°C. Energy dispersive spectroscopy (SEM Make, JEOL Model JSM - 6390LV, EDS Make JEOL Model JED - 2300), X-Ray diffraction (Bruker D8 Advance X-Ray diffractometer using Cu K $\alpha$  radiation), transmission electron microscopy (JEOL 3010 transmission electron microscope), micro-Raman (Jobin Yvon Horibra LABRAM-HR spectrometer using Ar<sup>+</sup> laser at 488nm as the excitation source), UV-Vis absorption (Shimadzu UV-2401PC spectrophotometer provided with an integrating sphere), and

photoluminescence (Hitachi model F-7000 FL spectrophotometer) measurements were carried out on the samples. The results of EDS analysis showed that the samples F1, F2, F5, F8, F15, F20 and F25 contained respectively 1.18 (1), 1.18 (2), 4.07 (5), 5.79 (8), 12.85 (15) and 20.32 (25) atom % of Fe (numbers within brackets indicate the atom % of Fe in the solution used for synthesis of Fe doped nanocrystalline TiO<sub>2</sub>) showing that a major part of iron in the starting solution got incorporated into the nanoparticles of TiO<sub>2</sub>. The photocatalytic activity of the undoped and doped nanocrystalline TiO<sub>2</sub> powders was studied by monitoring the degradation of the methylene blue dye in an aqueous solution (2 mg/L) containing the suspended nanocrystalline TiO<sub>2</sub> powders (0.4 g/L), under continuous stirring and exposure to visible light. The UV-visible spectra of each solution were recorded in the wavelength region 250 nm to 750 nm using JASCO UV-Visible spectrophotometer.

### Acknowledgements

The author M.A.K acknowledges the Kerala State Council for Science, Technology and Environment for granting a fellowship under Emeritus Scientist Scheme. The authors are thankful to IUC-DAE CSR, Indore, for providing facilities for XRD, TEM and micro-Raman measurements. Also, the authors thank STIC, Cochin University of Science and Technology for EDS measurements and NIIST, Thiruvananthapuram for DRS measurements.

Electronic supplementary information available: X-Ray diffraction patterns of samples (F15, F20\*, F25\* and F25), TEM micrographs of nanocrystals of TiO<sub>2</sub> containing 1 atom % and 2 atom % of iron, Micro-Raman spectra of samples F15, F20\*, and F25\*, and optical absorption spectra of iron doped nanoparticles of TiO<sub>2</sub>.

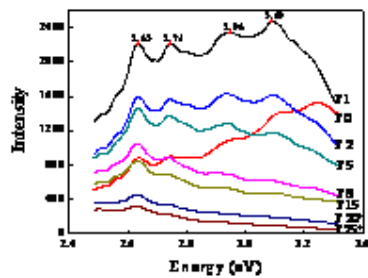
### References

- 1 I. Gur, N. A. Fromer, M. L. Geier, and A. P. Alivisatos, *Science*, 2005, **310**, 462-465.
- 2 X. Michalet, F. F. Pinaud, L. A. Bentolila, J. M. Tsay, S. Doose, J. J. Li, G. Sundaresan, A. M. Wu, S. S. Gambhir, and S. Weiss, *Science*, 2005, **307**, 538-544.
- 3 V. I. Klimov, S. A. Ivanov, J. Nanda, M. Achermann, I. Bezel, J. A. McGuire, and A. Piryatinski, *Nature*, 2007, **447**, 441-446.
- 4 Y. Cong, J. Zhang, F. Chen, M. Anpo, and D. He, *J. Phys. Chem. C*, 2007, **111**, 10618-10623.

- 5 X. H. Wang, J. G. Li, H. Kamiyama, M. Katada, N. Ohashi, Y. Moriyoshi, and T. Ishigaki, *J. Am. Chem. Soc.*, 2005, **127**, 10982-10990.
- 6 M. Hirano, T. Joji, and M. Inagaki, *Am. Ceram. Soc.*, 2004, **87**, 35-41.
- 7 M. Shim, and P. Guyot-Sionnest, *Nature*, 2000, **407**, 981-983.
- 8 C. Wang, M. Shim, and P. Guyot-Sionnet, *Science*, 2001, **291**, 2390-2392.
- 9 S. George, S. Pokhrel, Z. Ji, B. L. Henderson, T. Xia, L. Li, J. I. Zink, A. E. Nel, and L. Madler, *J. Am. Chem. Soc.*, 2011, **133**, 11270-11278.
- 10 X. Li, R. Wang, F. Zhang, and D. Zhao, *Nano Lett.*, 2014, **14**, 3634-3639.
- 11 I. S. Hwang, H. D. Kim, J. F. Kim, H. Y. Park, and H. Zim, *Phys. Rev. B.*, 1994, **50**, 8849-8852.
- 12 F. V. Mikulec, M. Kuno, M. Bennati, D. A. Hall, R. G. Griffin, and M. G. Bawendi, *J. Am. Chem. Soc.*, 2000, **122**, 2532-2540.
- 13 J. F. Suyver, S. F. Wuister, J. J. Kellya, and A. Meijerinka, *Phys. Chem. Chem. Phys.*, 2000, **2**, 5445-5448.
- 14 S. C. Erwin, L. Zu, M. I. Haftel, A. L. Efros, T. A. Kennedy, and D. J. Norris, *Nature*, 2005, **436**, 91-94.
- 15 G. M. Dalpian and J. R. Chelikowsky, *Phys. Rev. Lett.*, 2006, **96**, 226802.
- 16 D. M. Hoffman, B. K. Meyer, A. I. Ekimov, I. A. Merkulov, A. L. Efros, M. Rosen, G. Couino, T. Gacoin, J. P. Boilot, *Solid State Commun.*, 2000, **114**, 547-550.
- 17 D. J. Norris, N. Yao, F. T. Charnock, and T. A. Kennedy, *Nano Lett.*, 2001, **1**, 3-7.
- 18 C. A. Stowell, R. J. Wiacek, A. E. Saunders, and B. A. Korgel, *Nano Lett.*, 2003, **3**, 1441-1447.
- 19 M. Fujii, Y. Yamaguchi, Y. Takase, K. Ninomiya, and S. Hayashi, *Phys. Lett.*, 2005, **87**, 211919.
- 20 D. J. Norris, A. L. Efros, and S. C. Erwin, *Science*, 2008, **319**, 1776-1779.
- 21 Y. C. Cao, *Science*, 2011, **332**, 48-49.
- 22 R. A. Abram, G. J. Rees, and B. L. H. Wilson, *Adv. Phys.*, 1978, **27**, 799-892..

- 23 D. Mocatta, G. Cohen, J. Schattner, O. Millo, E. Rabani, and U. Banin, *Science*, 2011, **332**, 77-81.
- 24 J. D. Bryan, and D.R. Gamelin, *Prog. Inorg. Chem.*, 2005, **54**, 47-126.
- 25 T. A. Kennedy, E. R. Glaser, and P. B. Klein, *Phys. Rev. B*, 1995, **52**, R14356-R14359.
- 26 S. Sharma, S. Chaudhary, S. C. Kashyap, and S. K. Sharma, *J. Appl. Phys.*, 2011, **109**, 083905 1-7.
- 27 I. Ge, M. Xu, and H. Fang, *Thin Soild Films*, 2007, **515**, 3414-3420.
- 28 See Supplemental Material
- 29 B. D. Cullity and S. R. Stock, *Elements of X-ray diffraction*, Prentice Hall, USA, 2001.
- 30 X. Mathew, J. P. Enriquez, C. Mejía-García, G. Contreras-Puente, M. A. Cortes-Jacome, J. A. Toledo Antonio, J. Hays, and A. Punnoose, *J. Appl. Phys.*, 2006, **100**, 073907.
- 31 Y-H. Zhang and A. Reller, *J. Mater. Chem.*, 2001, **1**, 2537-2541.
- 32 J. Zhu, F. Chen, J. Zhang, H. Chen, and M. Anpo, *J. Photochem. Photobiol. A: Chem.*, 2006, **180**, 196-204.
- 33 G. Cao, *Nanostructures & Nanomaterials: Synthesis, Properties & Applications*, Imperial College Press, 2004.
- 34 G. Koutsoukos, A. N. Kofina, and D. G. Kanellopoulou, *Pure Appl.Chem.*, 2007, **79**, 825-850.
- 35 T. Ohsaka, F. Izumi, and Y. Fujiki, *J. Raman Spectro.*, 1978, **7**, 321-324.
- 36 D. Berdani, P.P. Lottice, and A. Montenero, *J. Mater. Sci.*, 2000, **35**, 4301-4305.
- 37 H. A. Szymanski, *Raman spectroscopy: Theory and Practice*, Plenum press, New York, 1967.
- 38 N. Serpone, and D. Lawless, *Langmuir*, 1994, **10**, 643-652.
- 39 K. Nagaveni, M. S. Hegde, and G. Madras, *J. Phys. Chem. B*, 2004, **108**, 20204-20212.
- 40 K. Das, S. N. Sharma, K. Mahesh, and S. K. De, *J. Phys. Chem. C*, 2009, **113**, 14783-14792.

- 41 M. Pal, U. Pal, J. M. Gracia, Y. Jiménez, Y., and F. Pérez-Rodríguez, *Nanoscale Res. Let.*, 2012, **7**, 1-12.
- 42 D. Beydoun, R. Amal, G. Low, and S. McEvoy, *J. Nanoparticle Res.*, 1999, **1**, 439-458.
- 43 M. R. Hoffmann, S. T. Martin, W. Choi, and D. W. Bahnemann, *Chem. Rev.*, 1995, **95**, 69-96.
- 44 D. P. Colombo and R. M. Bowman, *J. Phys. Chem.*, 1996, **100**, 18445-18449.



The phenomenon of 'self-purification' is a real mechanism operative in nanocrystals and this should be taken into account while doping semiconductor nanocrystals with external impurities for practical applications.